A multi-wavelength streaked optical pyrometer for dynamic shock compression measurements above 2500 K

Article *in* Review of Scientific Instruments · March 2020

DOI: 10.1063/1.5126123

8 authors, including:

Yekaterina P Opachich
Lawrence Livermore National Laboratory
59 PUBLICATIONS **732** CITATIONS
SEE PROFILE

Ryan Crum
Lawrence Livermore National Laboratory
19 PUBLICATIONS **47** CITATIONS
SEE PROFILE

Eric Dutra
National Security Technologies LLC
12 PUBLICATIONS **10** CITATIONS
SEE PROFILE

Hannah Laura Shelton
Lawrence Livermore National Laboratory
7 PUBLICATIONS **12** CITATIONS
SEE PROFILE

Review of Scientific Instruments

A multi-wavelength streaked optical pyrometer for dynamic shock compression measurements above 2500 K

Cite as: Rev. Sci. Instrum. **91**, 033108 (2020); https://doi.org/10.1063/1.5126123
Submitted: 30 August 2019 . Accepted: 08 March 2020 . Published Online: 23 March 2020

Y. P. Opachich, R. S. Crum, M. W. Daene, E. C. Dutra, H. N. Mehta, H. L. Shelton, P. Watts, and M. C. Akin

Review of Scientific Instruments ARTICLE scitation.org/journal/rsi

A multi-wavelength streaked optical pyrometer for dynamic shock compression measurements above 2500 K

Cite as: Rev. Sci. Instrum. 91, 033108 (2020); doi: 10.1063/1.5126123
Submitted: 30 August 2019 • Accepted: 8 March 2020 •
Published Online: 23 March 2020

Y. P. Opachich,[1,a] R. S. Crum,[1] M. W. Daene,[1] E. C. Dutra,[2] H. N. Mehta,[3] H. L. Shelton,[1] P. Watts,[1] and M. C. Akin[1]

AFFILIATIONS

[1]Lawrence Livermore National Laboratory, Livermore, California 94551, USA
[2]Nevada National Security Site, Livermore, California 94551, USA
[3]University of California Irvine, Irvine, California 92617, USA

[a]Author to whom correspondence should be addressed: opachich1@llnl.gov

ABSTRACT

This article presents a concept and implementation of a calibrated streaked spectral pyrometer (SSP) temperature diagnostic used in dynamically driven shock experiments on a two-stage gas gun. This system relies upon measuring the total system response using a tunable monochromator, a NIST-traceable calibrated power meter, and a SSP. The diagnostic performance is validated against previously measured temperatures of shock driven z-cut quartz at 99 GPa and 93 GPa. The results are found to agree with the literature to within 5% and are discussed in this manuscript. The experimental setup utilizes measurements from multiple SSP systems per sample, providing several independent measurements and substantially increasing confidence in the extrapolated shock driven sample temperature.

https://doi.org/10.1063/1.5126123

I. INTRODUCTION

High-pressure experiments performed on dynamic platforms such as light-gas guns and pinch machines generate multi-megabar sample pressure conditions. These dynamic experiments create short-lived high-pressure shock waves and allow practical insight into the effects of extreme conditions on a variety of materials. Experimentally measured properties such as pressure, temperature, and volume are used to determine the equation of state (EOS) of materials under extreme conditions. These parameters must be measured with high precision in order to ensure EOS accuracy, with the end goal of reliable identification of boundaries between phase transitions and material response at extreme conditions.

While pressure and volume measurements with errors on the order of 1% have been regularly achieved,[1,2] this level of precision in the temperature measurement remains elusive. The existing research in shock physics heavily relies on the Mie–Grüneisen equations of state that are assumed true for the dynamically compressed material and used to provide an estimate of the sample's bulk temperature.[3] Models with differing assumptions lead to equations of state that are similar in pressure and volume but disagree in temperature.[4] This assumption provides an approximation of temperature, and experimentally measured data are necessary to verify and improve the accuracy of equations of state of many materials.

In gas gun experiments, temperature is typically measured with pyrometry.[5] This is a technique that records optical self-emission from the shocked material to infer the surface temperature for opaque materials and bulk for those that are transparent. Much of the data currently in the field are collected with optical or near infrared pyrometer systems that consist of 4–6 narrow band-pass (10–40 nm width) filter channels that are coupled to either a photomultiplier tube or a diode. Temperature is determined by fitting the recorded intensity of each channel to a blackbody function; subsequently, the accuracy of the fit depends on the bandwidth and number of channels over the experimental emission range. In addition, the spectral response of each channel must be well understood. Calibration of optical pyrometers requires a well characterized

photon source, which is treated as a graybody of known emissivity and temperature. Unfortunately, accurate calibration is challenging due to the fact that commonly used sources such as tungsten ribbon lamps[3] or coiled-coil irradiation lamps[6] do not cover the experimental temperature range greater than 3000 K. In addition, calibration sources can degrade over time in many ways: W can be deposited on the bulb, acting as a filter; resistance of the filament can change, leading to a different T for a given input current; or the surface emissivity can change over time. These sources also produce spatially nonuniform radiation, introducing uncertainty into the temperature measurements. In propagating subsequent uncertainties, this conventional treatment introduces many errors that must be considered. These are especially notable in the shorter wavelengths, where typical sources provide very little light. Here, we present a calibration technique that eliminates this uncertainty and extends the calibration temperature range above 2500 K by utilizing a well characterized, tunable monochromatic light source with photon flux comparable to experimental conditions.

More recently, streaked optical pyrometry (SOP) has been used in laser-driven experiments to measure high temperatures with a fast temporal response.[7–10] This method can provide unfiltered total emission brightness on a single streak camera (SC) record[7] and emission over a specific bandwidth after the introduction of bandpass filters.[8,9] These diagnostics typically have one or two channels. In this work, we modified the streaked optical pyrometry measurement technique to collect the temporally resolved emission spectra by introducing a grating before the input slit of the streak camera detector. The grating spectrometer provides a wide spectral range of independent temperature measurements over a single temporally dispersed (swept) image. The total number of spectral elements in such a system is set by the combination of the spectral resolution of the grating and the spatial resolution of the streak camera (see Fig. 1). Our system has an equivalent of ~150 nm, 2 nm wide, spectral elements over the 400–700 nm emission range. This is a sizable increase in comparison to the spectral coverage that is available with an optical pyrometer or SOP. Because we calibrate the detector response over each spectral element, variations in emission due to emissivity or band emission can be better detected than with conventional pyrometry, which integrates over larger bands. The spectral power response of all of our streaked spectral pyrometer (SSP) systems was calibrated using static narrow-band emission from several light sources (LEDs, ribbon lamps, and other bright lamps). To generate the monochromatic source, a wavelength was bandwidth selected with a double-slit monochromator. This setup essentially eliminates the need to have a source of known temperature and enables the use of shorter wavelengths for calibration. Late time emission from an additional Xe light source was also used to provide Xe spectral emission lines, which were used for wavelength calibration, and to monitor the overall spectral resolution of the SSP before and after each experiment. To validate the diagnostic performance, two SSP systems were fielded on a dynamically compressed quartz experiment that has been studied extensively. The temperature measurements were within 3% agreement among the diagnostics and showed within 5% agreement with the previous results of Lyzenga *et al.*[3] and Boslough.[11]

This work aims to lower the uncertainty in the inferred shocked sample temperature by using multiple streaked spectrometer cameras, a Xe flash source, narrow-band spectral power

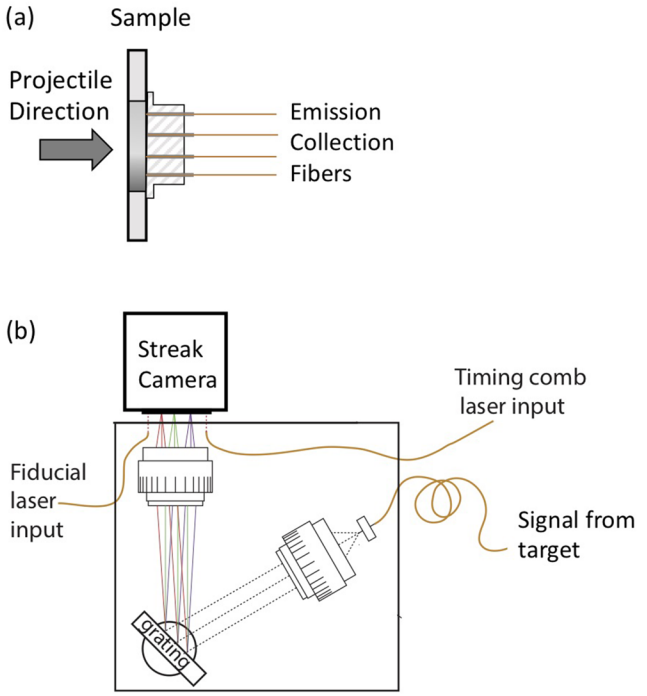

FIG. 1. (a) A diagram of the experimental setup. Up to four fibers are used to collect emission from the sample. The 300 μm core fibers are fed through the gas gun chamber walls, where they are stepped down to a 50 μm fiber-optic system and input into the SSP detectors. (b) Components of the SSP detector. Self-emission from the sample is relayed onto the grating and then refocused onto the streak camera slit with Nikon lenses. In addition, a t_0 timing fiducial and a timing comb are recorded during the shot to synchronize the four SSP systems to the experiment and to calibrate the temporal data axis, respectively.

measurements, and a dynamically compressed quartz sample for cross-calibration. In addition to the use of several SSP systems and a slight change to our experiment setup, we can measure the wavelength-dependent emissivity functions of materials. When two streaks are coupled such that one can measure a reflected source while the other measures radiance, we can calculate the wavelength-dependent emissivity function. This function is crucial to improve pyrometry; as in conventional graybody pyrometry, the function is assumed to be wavelength independent and treated as a fitting parameter. Finally, the utilization of a tunable monochromatic source during calibration and *in situ* measurements from multiple streaked spectrometer detectors allow this process to potentially outperform the accuracy of traditional multichannel pyrometers and pyrometer calibration methods.

II. EXPERIMENTAL CONFIGURATION

A typical target used in our gas gun experimental setup is shown in Fig. 1(a). Self-emission from the sample is collected by target-mounted, un-lensed 300 μm core fibers that are 2 m long, which are replaced with each shot. These fibers are mated at the gas gun tank to a permanent external 40 m long, 50 μm core visible fiber using a Straight Tip (ST) connector, effectively reducing the collecting area of the system to that of the 50 μm fiber. Our target design

allows, but is not limited to, four sample probe locations that are input into independent SSP detectors.

The SSP spectrometer, shown in Fig. 1(b), is essentially of the Czerny–Turner type, with mirrors replaced with achromatic Nikon, Nikkor 105 mm f/2D lenses. The output from the 50 μm target fiber is expanded onto the Richardson plane ruled 300 gr/mm grating via the first lens. The first-order diffracted signal is then focused to ~50 μm onto the streak camera photocathode. A timing comb and an experimental t_0 fiducial are input at the edges of the camera slit for detector synchronization and to provide an accurate measure of the temporal axis in the recorded streaks. The optical streak camera (SC) was built by the Nevada National Security Site (NNSS); see Fig. 2 for a schematic representation. The camera utilizes a P-20 gated cathode to convert the photon signal to electrons that are then extracted and accelerated through a slit and anode. The effective slit size is 1 mm. The electron beam is then swept and focused onto a fiber optic bundle that is coated with S-20 phosphor and a thin Al layer. The output from the streak camera is amplified with a Micro Channel Plate Intensifier (MCPI) and fiber coupled into a Spectral Instruments SI-800 CCD camera that is equipped with a 9 μm 4096-by-4096-pixel imaging chip. This custom-built camera provides user selectable sweep speeds that range from 2 μs to 10 μs.

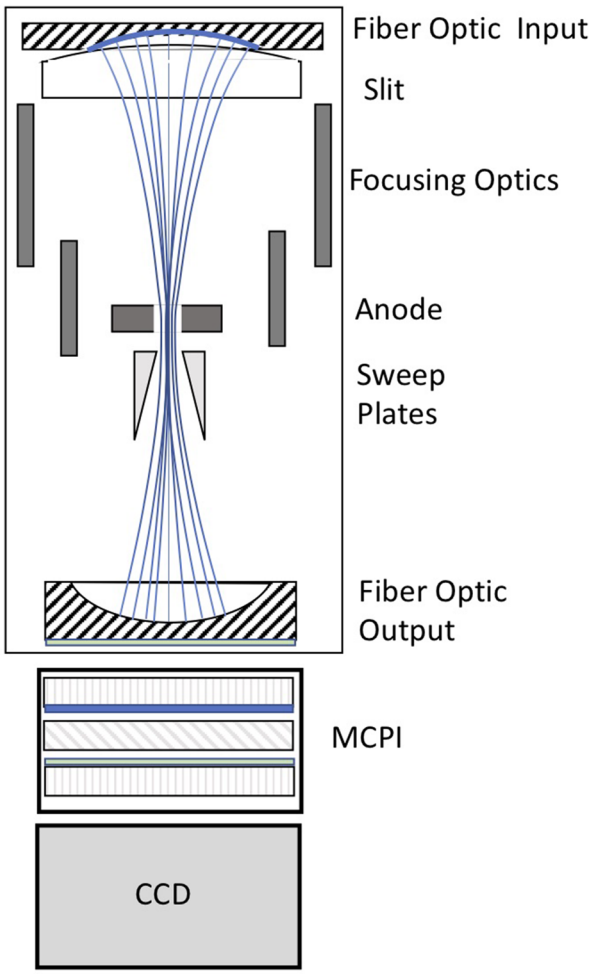

FIG. 2. Diagram showing the components of the NNSS streak camera. Light from the monochromator is focused onto the slit located in the fiber optic input (top of the image). A P-20 photocathode then converts the photon signal to electrons. The electrons are extracted away from the photocathode, where they are focused and deflected by the focusing optics and sweep plates onto the fiber optic output bundle. Here, the swept electrons are converted to a visible light image with an S-20 phosphor coating. The MCPI amplifies the phosphor signal, and the CCD records the resulting image.

During shot execution, the spectral image, timing comb, and fiducial are captured in a single image, as shown in Fig. 3. Sweep rates for each camera are set independently; for the majority of experiments, we have used a 2 μs sweep (cameras SSP1, SSP2, and SSP4) and a 712 ns sweep (camera SSP3) to provide increased temporal resolution.

The image $\mathbf{M}(x, y)$ (see Fig. 3), where x denotes the image row pixel and y denotes the image column pixel, is integrated over a given time window of interest and processed for baseline removal to generate a series of intensity spectra $I(\lambda, t)$ with units of counts s^{-1} m^{-1}, where λ is wavelength and t is time. $I(\lambda, t)$ is divided by the camera response function $K(\lambda)$ to yield a spectral power function $P(\lambda, t)$ with units of W m^{-1}. The spectral power $P(\lambda, t)$ is related, in turn, to the spectral radiance $L(\lambda, t)$ as

$$P(\lambda, t) = \tau(\lambda)\, \pi A \sin^2(\vartheta) \mathcal{E}(\lambda, t) L(\lambda, t), \tag{1}$$

where $\tau(\lambda)$ is the transmission fraction at the quartz-vacuum interface, A is the collection area of the fiber (1.96×10^{-9} m^2), and $\sin^2(\vartheta)$ is the solid angle determined by the fiber's numerical aperture (NA). $\mathcal{E}(\lambda, t)$ is the emissivity function, given by Kirchoff's law as $(1 - R(t))$, where $R(t)$ is the reflectivity of the sample at time t. $L(\lambda, t)$ is Planck's

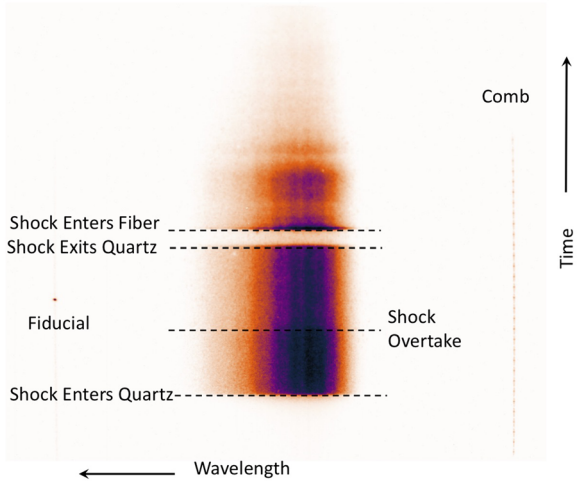

FIG. 3. Streaked spectroscopic data collected from a 6.4 mm-thick z-cut single-crystal quartz shocked to 99 GPa and 93 GPa with SSP2. The target was designed to create two different shock states. Because quartz emits from the shock front, these two states can be clearly seen by the change in brightness that occurs about halfway through the transit. A fiducial marker is placed on the left and a timing comb on the right for cross-timing.

law applied in the fitting algorithm with units of $\mathrm{Wsr}^{-1}\ \mathrm{m}^{-3}$ defined as

$$L(\lambda, t) = \frac{2hc^2}{\lambda^5} \frac{1}{e^{\frac{hc}{\lambda k T(t)}} - 1}, \tag{2}$$

where h, c, and k are Planck's constant, the speed of light, and Boltzmann's constant, respectively, λ is in meters, and T is in kelvin. To obtain high-quality measurements and fit $L(\lambda, t)$, we must determine time and wavelength as a function of pixel $t(y)$, $\lambda(x)$, along with $K(\lambda)$, A, NA, $\tau(\lambda)$, and $\mathcal{E}(\lambda, t)$ in detail. Typically, A, NA, $\tau(\lambda)$, and $\mathcal{E}(\lambda, t)$ are measured independently, while $t(y)$, $\lambda(x)$, and $K(\lambda)$ are dependent on the diagnostic performance. The calibration methodology discussed in Secs. III A–III E served to fully calibrate the SSP diagnostics in order to accurately determine the sample temperature from the dynamically compressed experimental data.

III. CALIBRATION

The performance of the streaked spectral pyrometer diagnostics was characterized at the NNSS (Livermore Operations) and at the Lawrence Livermore National Laboratory (LLNL). The complete SSP calibration included a measurement of the diagnostic's sweep speed, temporal and spatial resolution, magnification, spectral response, spectral resolution, gain, and wavelength calibration. The details of each measurement are summarized in Subsections III A–III E, and calibration results for all SSP systems are presented in Table I.

A. Sweep speed and temporal resolution

The streak camera temporal resolution and sweep speed were determined by using a 650 nm, 20 MHz (50 ns inter-pulse spacing) optical comb generator. The pulse duration and separation of the comb generator output are highly repeatable, making this source optimal for calibration. The streak camera sweep speed was calculated from the temporal separation of each pulse in the swept image along the center and top regions of the CCD. To determine a functional relationship $t(y)$ between the image pixel and time, a lineout was taken across the pulse train in the swept image (Fig. 3). The resulting profile was fit with the *findpeaks* function in MATLAB to identify the y position of the timing-comb peaks. The final time vs pixel plot is shown in Fig. 4(b). The data closely follow a linear fit, showing that the sweep speed is uniform to ±2.5 ns across the CCD.

Temporal resolution along the center of the swept streak camera image was calculated by measuring the full width at half maximum (FWHM) of individual optical pulses. The average temporal resolution of the slow sweep (2 μs window) streak spectrometer systems is ~18.8 ns at FWHM. The fast (712 ns window) streak spectrometer system has a temporal resolution of ~2.9 ns FWHM.

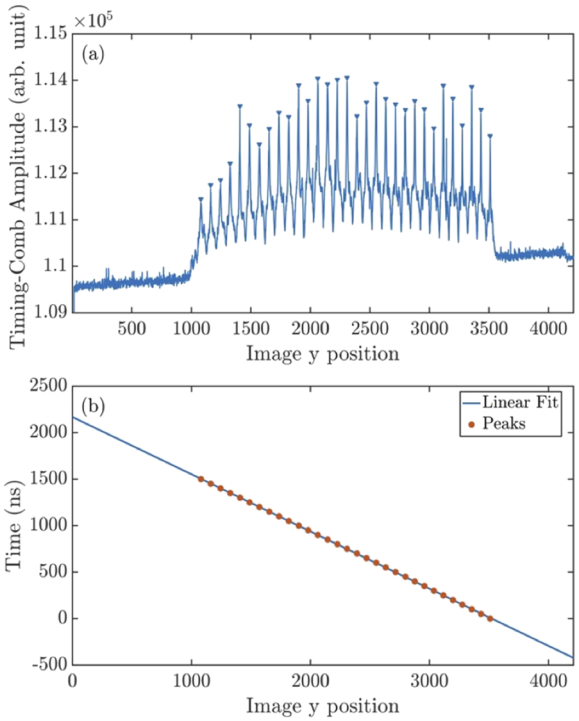

FIG. 4. (a) A profile of timing-comb amplitude vs image y position is computed by integrating in the t direction over a thin band containing the timing-comb in the raw image. The peaks are automatically identified, and the relative times are determined using the known 50 ns spacing of the timing comb. (b) The times and y positions of the peaks are used to calculate a linear fit for $t(y)$, which is a time axis to each row y of the image.

B. Spatial resolution and magnification

The streak camera spatial resolution and the magnification contribute to the overall spectral resolution of the SSP diagnostic. To determine both the spatial resolution and magnification of the diagnostics, we used a PR-10 300 μm resolution Optoliner® system from Davidson Optronics. The system uses a spatial resolution pattern, with several groups of vertical bars of known thickness and separation. The pattern is placed on the Optoliner flashlamp system

TABLE I. Streak camera calibration results summary.

Streak spectrometer system	Temporal resolution FWHM (ns)	Sweep speed (mm/ns)	Spatial resolution (lp/mm)	Magnification (times)	λ to pixel ratio (nm/px)
1 (2 μs)	18.8	0.0198	18.3	1.01	0.27
2 (2 μs)	19.8	0.0203	18.3	1.01	0.29
3 (712 ns)	2.98	0.0563	18.3	1.01	0.28
4 (2 μs)	17.8	0.0195	18.3	1.01	0.28

and focused onto the streak camera. An example of the swept pattern is shown in Fig. 5. The dark regions correspond to the mask bars; the recorded bar width is used to calculate the magnification and swept spatial resolution of the detector. The measured spatial resolution of our cameras is ~18.3 line pairs per mm (lp/mm), with a magnification of 1.01 times. This was determined by the best resolve bar in the image and the corresponding lp/mm of the pattern.

C. Spectral response

The spectral response, $K(\lambda)$, of the SSP was calibrated with a tunable, monochromatic (~2 nm FWHM) source in the visible range covering 400–700 nm. To do this, either a coiled-coil lamp, halogen lamp, or LED source was focused onto a large (>600 μm) core optical fiber such that it was over-filled. The output of this fiber was inserted into a double-slit monochromator, where the source wavelength was selected in steps of 5 nm. The spectral content at the output of the monochromator was verified to be about ~2 nm FWHM with an Ocean Optics USB-2000 spectrometer. This narrow-band light was focused onto a 2 m long, 50 μm core ST optical fiber using a 10× objective lens. The signal from the 2 m long fiber was then input into the entrance slit of the SSP, where it was spectrally dispersed and refocused onto the streak camera photocathode. The setup is summarized in Fig. 6. The power input into the SSP was measured with a NIST-certified power meter and detector system (Newport 2936RR meter and Newport 918D-UV-OD Si Detector). When operated in continuous mode, as we do, this meter is accurate to 0.2% according to the manufacturer's specifications, while the detector is calibrated to 1% accuracy. All meters and detectors were calibrated specifically for this project and background corrected. The typical measured output was ~64 μW/cm^2.

We found that the measured power level of the monochromator output was too low to be detected when the streak camera was set to disperse signal temporally, so all data points were collected in static mode (no voltage ramps at the sweep plates). To temporally gate the signal, the streak camera photocathode utilized a ~13 μs "on" gate, with a 2 s CCD exposure. The SSP was connected to a DG 535 for an external trigger source and an oscilloscope to verify the gate duration. Three streak camera images were recorded at each wavelength. The CCD count data from the recorded gated images were divided by the input energy values to create a camera response curve in counts/J, as shown in Fig. 7. The data were fit with a cubic spline fit as a function of wavelength.

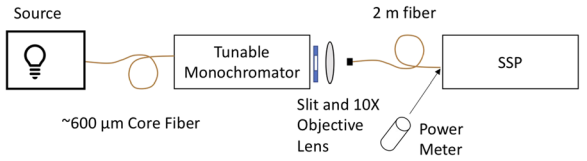

FIG. 6. Spectral response measurement setup. An optical light source (either a coiled-coil lamp, halogen lamp, or LED) is used to generate a visible light spectrum. Output from the source is focused onto a 600 μm core fiber and input into a tunable monochromator. A narrow, ~ 2 nm spectral band is selected at the output of the monochromator and focused into a 2 m long fiber and fed into the SSP. A power meter was used to characterize the power of the signal that is input into the SSP.

D. Gain calibration

The gain of each camera is set independently by adjusting the streak camera MCPI voltage. The systems are designed such that each 50 V increase in the MCPI will roughly double the gain. The MCPI gain is given by

$$G(V_{MCPI}) = 10^{-a+bV_{MCPI}}, \tag{3}$$

where G is the gain and V_{MCPI} is the MCPI voltage setting in volts. The data from each camera are fit using the gain Eq. (3) because gain varies from system to system. Un-swept images were collected at gain settings in 50 V increments ranging from 500 V to 950 V. The output of the tunable monochromator was set to select a wavelength centered at 525 nm and input into the SSP. The average power incident into the SSP entrance slit was ~6.8 nW and varied by ±2 pW. The average counts in the spectrally dispersed fiber spot were plotted

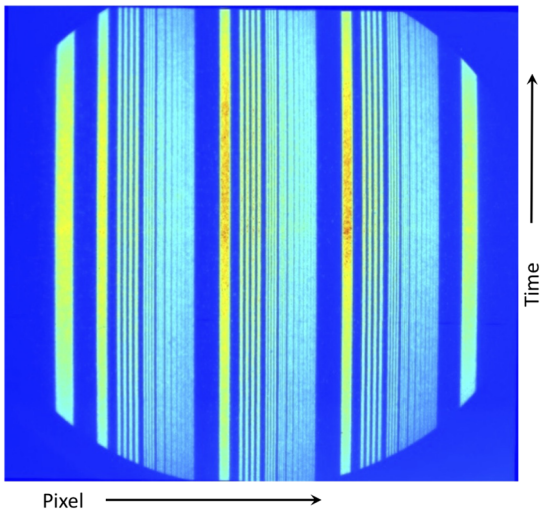

FIG. 5. Example of a swept spatial resolution pattern. Dark (blue) regions correspond to the projected shadow of the masked regions.

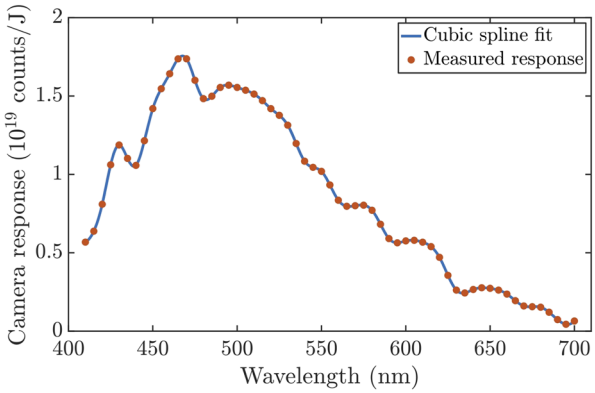

FIG. 7. An example of the measured camera response curve for SSP2. Measurement points (closed red) and spline fitted data (blue curve).

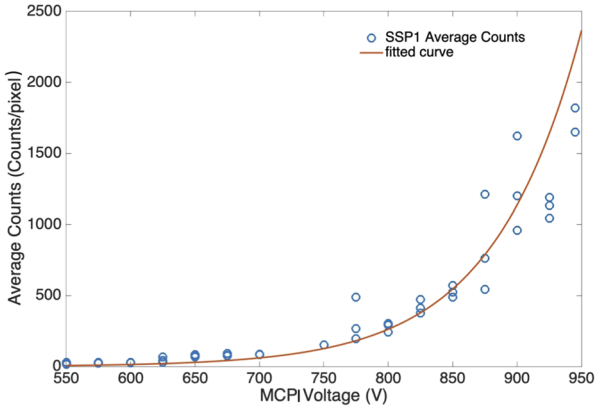

FIG. 8. An example of a gain curve and fit. Here, the average counts of the spectrally dispersed spot on the CCD are plotted as a function of voltage. The resulting fit parameters were a = 2.674, b = 0.006 367 with an R-squared value of 0.7857.

as a function of MCPI voltage and then fit (Fig. 8). The fit follows the collected data closely at lower voltages. At higher voltages, the MCPI begins to saturate showing greater deviation from the fit.

E. Spectral resolution and wavelength calibration

The spectral resolution and wavelength assignment were calibrated before and after each experiment using emission from a Xe flash lamp for all SSP diagnostics. An example of the recorded swept Xe spectrum is shown in Fig. 9(a). A lineout of the data was taken to generate the Xe emission spectrum shown in Fig. 9(b). Peaks were matched to the lines from the NIST Atomic Spectra Database (NIST_ASD) and used to assign a spectral axis, i.e., wavelength as a function of horizontal pixel position [$\lambda(x)$], to the image. First, the six persistent lines of singly ionized Xe between 484 nm and 610 nm were matched to peaks in the integrated spectrum, and additional lines, when clearly identifiable, were used to refine the fit. Again, we found that linear fits for $\lambda(x)$ were sufficient to describe the relation between the Xe line wavelength and the image x position on all cameras. The collected spectra also show that the spectral resolution of the SSP diagnostics was <2 nm, as shown in the resolved 439 nm doublet in Fig. 9(b). Due to alignment variations, each camera has a slightly different wavelength-to-pixel ratio, ranging from 0.27 to 0.29, as summarized in Table I.

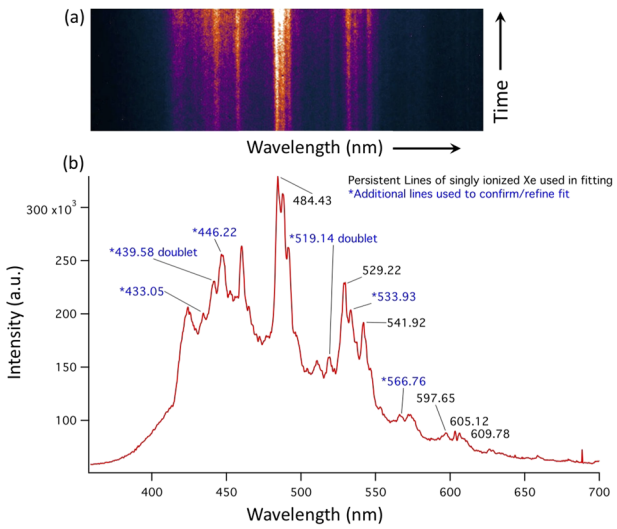

FIG. 9. Example of measured Xe flash emission for SSP 1 (shot 4291). A lineout is taken across (a) to generate a spectrum shown in (b). The spectrum is used to assign the wavelength to the emission data. Six major peaks between 484 nm and 610 nm are used in the initial fits for all camera systems. Additional peaks marked with $*$ are used to refine the wavelength assignments.

IV. TEMPERATURE OF SHOCKED QUARTZ

The performance of two SSP diagnostics was validated on a dynamically compressed z-cut Quartz experiment, and the results were compared to previously reported temperatures at similar experimental conditions. Quartz was chosen for several reasons: The behavior of shock driven quartz has been extensively studied.[3,11–13] The material is transparent, and emission is generated in the bulk of the sample by an opaque shock front within the material.[3] In addition, consistent pure samples are readily available. The experiments were performed on a two stage gas gun at the High Explosives Applications Facility (HEAF) located at the Lawrence Livermore National Laboratory. The sample consisted of a ~6.4 mm thick by 38 mm diameter, z-cut single-crystal quartz, mounted on a 1.500 mm Al-1100 baseplate. The target was impacted by using a 2.005 mm Cu impactor at 5.77 km/s. This design allows us to test two shock states in quartz. An example of the resulting SSP data is shown in Fig. 3. The shock enters the quartz sample, initiating optical emission; the sample is at a pressure of 99 GPa; and at this early time, it is in a superheated solid state. A lower-pressure reverberation with the Cu impactor and Al baseplate overtakes the first shock about halfway through the sample, causing the temperature to drop. This new shock state is ~93 GPa, and the decreased temperature can be clearly seen in the image. The shock exits the quartz and emission ceases; at this point, the experiment is over. The secondary late time increase in emission in the observed streak image is due to the shock entering the collection fiber.

V. RESULTS AND DISCUSSION

In order to calculate a temperature from the streaked spectrometer image, datasets collected by both SSP systems were background subtracted. Temporal and spectral axes were assigned to the images

TABLE II. Calculated mean temperatures and uncertainties for a z-cut quartz crystal from SSP1 and SSP2 (shot 4246). Uncertainties include the standard deviation in the calculation and wavelength assignment for each camera.

Camera	Pressure (GPa)	Temperature (K)
SSP1	99	5461 ± 55
	93	5261 ± 56
SSP2	99	5465 ± 40
	93	5302 ± 54

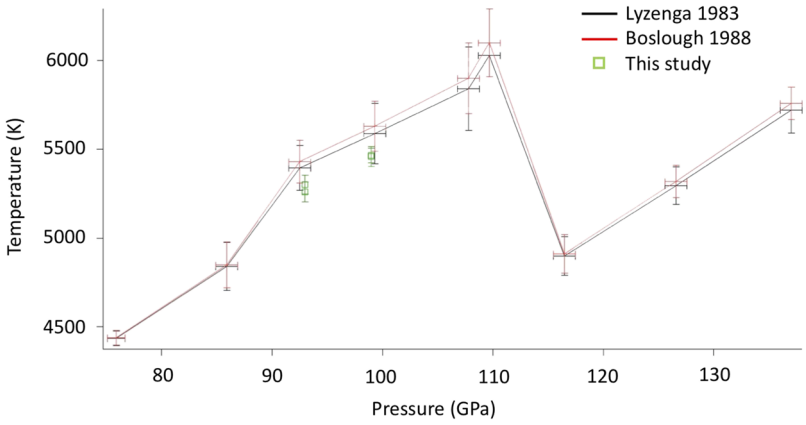

FIG. 10. Calculated temperatures from detectors SSP1 and SSP2 compared to those published by Lyzenga *et al.*[3] and reanalyzed by Boslough.[11] Our measurement is within 5% agreement with the previously published data.

from the recorded fiducial, comb, and Xe spectra. The images were scaled to account for the MCPI gain settings used to collect shot data, and the response curves were used to convert the counts recorded on the CCD to units of power. The corrected streaked spectral emission data were then integrated with respect to time to yield spectral power. Temperature was determined by fitting the power spectra with a graybody equation; the details of the data analysis process, error sensitivities, and additional quartz temperature measurements are partially summarized in our recent publication[14] and will be the focus of future publications.

Quartz sample temperatures were determined by averaging over the fit at 99 GPa and 93 GPa for each dataset. The results are shown in Table II. Sample pressure as a function of time was inferred from a separate *in situ* Photon Doppler Velocimetry (PDV)[15] measurement. Both the PDV and SSP timing were cross correlated with a fiducial generated by the gas gun. Uncertainty includes the standard deviation from the graybody fit, along with uncertainty due to wavelength assignment, which is about ±38 K for SSP1 (comparable to the fitting uncertainty) and ±15 K for SSP2. We compare these to the measurements of Lyzenga *et al.*[3] and Boslough,[11] and find them to agree well (within 5%), as shown in Fig. 10. Uncertainty in the reported temperature was calculated as the quadrature sum of the fitted graybody curve and uncertainty in wavelength alignment. Wavelength alignment was calculated to have an uncertainty of about 2 nm due to the combined effects of small rotations of the detector relative to the streak, camera focus, and peak fitting of the spectra. Modeling the effect of this misalignment showed that about 10 K uncertainty was introduced for each nm of misalignment, so we estimate the uncertainty due to potential misalignment to be 20 K. We plan to write up the details of our error analysis and explore additional possible error sources in a future manuscript. In addition, a manuscript describing the quartz measurements in more detail has been submitted to the 2019 Shock Compression of Condensed Matter (SCCM) AIP conference proceedings.

VI. CONCLUSIONS AND FUTURE WORK

We have presented an alternate method of inferring temperature from temporally and spectrally resolved emission data collected with a calibrated streaked spectral pyrometer diagnostic in dynamically driven shock experiments. The diagnostic was fully calibrated; in addition, the spectral response of the system was characterized with the use of a tunable, monochromatic light source. This enables any light source to be used and extends the current calibration range. The performance of two systems was validated with a dynamic measurement of shocked quartz emission and compared to the previously measured data. The measured temperature was within 5% agreement with other methods in use, while the temperature inferred from the two systems was within ~1%. Future work will involve examining the reproducibility of this procedure, additional quartz measurements, performing experiments at higher and lower temperatures, and using our calibrated systems to directly measure the wavelength-dependent emissivity function of materials undergoing dynamic compression to improve temperature calculations.

ACKNOWLEDGMENTS

We thank Gerard Jacobson, Bob Nafzinger, Paul Benevento, Eric Shi, Sam Weaver, Ryan Kelley, Anthony Mendez, Paul Dealmeida, and Cory McLean for their dedicated effort.

This work was performed under the auspices of the U.S. Department of Energy by the Lawrence Livermore National Laboratory under Contract No. DE-AC52-07NA27344.

This manuscript has been authored by Mission Support and Test Services, LLC, under Contract No. DE-NA0003624 with the U.S. Department of Energy, National Nuclear Security Administration, Office of Defense Programs. The views expressed in the article do not necessarily represent the views of the U.S. Department of Energy or the United States Government (Grant No. DOE/NV/03624—0447).

REFERENCES

[1] N. C. Holmes, J. A. Moriarty, G. R. Gathers, and W. J. Nellis, J. Appl. Phys. **66**(7), 2962 (1989).
[2] M. C. Akin, J. H. Nguyen, M. A. Beckwith, R. Chau, W. P. Ambrose, O. V. Fat'yanov, P. D. Asimow, and N. C. Holmes, J. Appl. Phys. **125**, 145903 (2019).
[3] G. A. Lyzenga, T. J. Ahrens, and A. C. Mitchell, J. Geophys. Res.: Solid Earth **88**(B3), 2431, https://doi.org/10.1029/jb088ib03p02431 (1983).
[4] P. C. Myint, E. L. Shi, S. Hamel, H. Cynn, Z. Jenei, M. J. Lipp, W. J. Evans, and M. C. Akin, J. Chem. Phys. **150**(7), 074506 (2019).
[5] *Treatise on Geophysics*, edited by P. D. Asimow and G. Schubert (Elsevier, Oxford, 2015), pp. 393–416.

[6]O. V. Fat'yanov and P. D. Asimow, Rev. Sci. Instrum. **86**, 101502 (2015).
[7]J. E. Miller, T. R. Boehly, A. Melchior, D. D. Meyerhofer, P. M. Celliers, J. H. Eggert, D. G. Hicks, C. M. Sorce, J. A. Oertel, and P. M. Emmel, Rev. Sci. Instrum. **78**, 034903 (2007).
[8]D. K. Spaulding, D. G. Hicks, R. F. Smith, J. H. Eggert, R. S. McWilliams, G. W. Collins, and R. Jeanloz, in *Shock Compression of Condensed Matter – 2007*, edited by M. Elert, M. D. Furnish, R. Chau, N. Homes, and J. Nguyen (American Institute of Physics, 2007), pp. 1071–1074.
[9]T. Morita, Y. Sakawa, Y. Kuramitsu, H. Tanji, H. Aoki, T. Ide, S. Shibata, N. Onishi, C. Gregory, A. Diziere, J. Waugh, N. Woolsey, Y. Sano, A. Shiroshita, K. Shigemori, N. Ozaki, T. Kimura, K. Miyanishi, R. Kodama, M. Koenig, and H. Takabe, Astrophys. Space Sci. **336**(1), 283–286 (2011).
[10]E. Floyd, E. T. Gumbrell, J. Fyrth, J. D. Luis, J. W. Skidmore, S. Patankar, S. Giltrap, and R. Smith, Rev. Sci. Instrum. **87**, 11E546 (2016).
[11]M. B. Boslough, J. Geophys. Res. **93**(B6), 6477, https://doi.org/10.1029/jb093ib06p06477 (1988).
[12]D. G. Hicks, T. R. Boehly, J. H. Eggert, J. E. Miller, P. M. Celliers, and G. W. Collins, Phys. Rev. Lett. **97**, 025502 (2006).
[13]R. S. McWilliams, Ph.D. thesis, University of California, Berkeley, 2008.
[14]H. L. Shelton, Y. P. Opachich, H. N. Mehta, R. S. Crum, E. Dutra, E. L. Shi, and M. C. Akin, in Proceedings of SCCM, 2019.
[15]O. T. Strand, D. R. Goosman, C. Martinez, T. L. Whitworth, and W. W. Kuhlow, Rev. Sci. Instrum. **77**, 083108 (2006).